Available online at www.sciencedirect.com
SCIENCE DIRECT
Journal of Crystal Growth 288 (2006) 218–224
JOURNAL OF CRYSTAL GROWTH
www.elsevier.com/locate/jcrysgro

InN: A material with photovoltaic promise and challenges

Elaissa Trybus[a], Gon Namkoong[a], Walter Henderson[a], Shawn Burnham[a], W. Alan Doolittle[a,*], Maurice Cheung[b], Alexander Cartwright[b]

[a]School of Electrical and Computer Engineering, Georgia Institute of Technology, 777 Atlantic Dr., Atlanta, GA 30332, USA
[b]University at Buffalo, State University of New York, Buffalo, NY 14260, USA

Abstract

The potential of InN as a photovoltaic material is described. For solar applications, several key developments such as p-type doping and solid-state rectifying junctions have yet to be demonstrated. However, the ability of InGaN materials to optimally span the solar spectrum offers a tantalizing solution for high-efficiency photovoltaics albeit in an inherently lattice mismatched material system. For this reason, the characteristics of InN grown on (1 1 1)-oriented germanium and (0 0 0 1)-plane sapphire substrates via molecular beam epitaxy for the application of InN solar cells is described. To provide an efficient sub-cell interconnect for tandem solar cells, epitaxial Al was deposited on a germanium substrate with InN grown on this epitaxial aluminum layer. Consistent with previous results, the electrical characteristics of n-InN/p-Ge, n-InN/n-Ge, and n-InN/Al/Ge were measured and showed no rectifying behavior. As evidenced by X-ray diffraction, minute amounts of unintentional oxygen incorporation during InN growth forms a secondary phase, tentatively assigned to an indium oxynitride, $InON_x$, phase. Photoluminescence measurements of the InN/$InON_x$ show spectral peaks at ~0.7 and ~3.8 eV consistent with the bulk excitonic bandgap of the two materials. Photoluminescence was also found at ~1.7 eV and shown to be related to emission from the sapphire substrates.

PACS: 81.15.Hi; 78.66.Fd; 61.10.Nz

Keywords: A1. X-ray diffraction; A3. Molecular beam epitaxy; B3. Semiconducting III–V materials; B3. Solar cells

1. Introduction

The revised bandgap value of InN [1–3] has attracted global attention due to new technology opportunities for the implementation of high-efficiency InN photovoltaic (PV) devices. However, there remains debate about the bandgap, specifically the origin of the larger bandgap [4,5] and its relation to oxygen-compound and bandfilling effects [6,7]. Despite this debate, the development of InN solar cells remains a significant focus.

The current state-of-the art solar cell has an efficiency greater than 35% and was fabricated from lattice-matched III–V semiconductors on a germanium (Ge) substrate [8]. Ge substrates provide adequate lattice matching to InN compared to traditional substrates such as sapphire [3]. Ge also allows for a vertical conduction device design that can reduce shadow losses leading to higher efficiencies compared with top-connected solar cells. However, Ge substrates have not been explored by group III-nitride materials experts because of impediments to growth that have been technically difficult to overcome. Georgia Institute of Technology has demonstrated the successful growth of InN on Ge substrates [3]. This demonstration may allow for increased flexibility in the design of novel InN solar cells.

A current challenge to InN PV devices is strong band bending [9–11] at the surface/heterointerface, which so far has resulted in the inability to form a rectifying solid-state junction. Specifically, the strong band bending at the collecting junction prevents the collection of minority carriers, leading to ohmic junctions through the tunneling mechanism. If the background doping in InN could be substantially lowered, such band bending near the surfaces

*Corresponding author. Tel./fax: +1 404 894 9884.
E-mail address: alan.doolittle@ece.gatech.edu (W.A. Doolittle).

0022-0248/$ - see front matter © 2006 Published by Elsevier B.V.
doi:10.1016/j.jcrysgro.2005.12.120

could be beneficially used as an efficient means of reducing surface recombination via re-direction of minority carriers away from the defective surfaces.

Another challenge to InN PV device development is that p-type doping of InN has yet to be demonstrated. p-type doping is needed to create the p–n sub-cell collecting junction and for the degenerately doped interconnect regions. The p–n collecting junction facilitates current collection through the electrostatic field created by the spatially separated ionized donors and acceptors. Without such p–n junctions, photogenerated electron hole pairs cannot be separated, therefore no photocurrent is produced. Additionally, traditional tandem solar cells use degenerately doped materials at the sub-cell junctions to facilitate tunnel junctions. In this region the conduction and valence band of the materials overlap, allowing the electrons collected at the sub-cell p–n junctions to tunnel from the n-type emitter of one sub-cell into the neighboring holes in the adjacent sub-cell base. Without p-InN, an InN PV tandem device will need a substantially different means of current collection, such as an internal Schottky barrier or heterojunction for current collection. InN PV tandem devices will also need an alternative means of sub-cell interconnect, independent of the tunneling between degenerate layers. Otherwise, the photogenerated electron hole pairs will not result in current in the external circuit.

Herein, this article details a few challenges and possible solutions for InN solar cell devices; and presents data to aid in the discussion on the discrepancy between the bandgap values of InN. The growth and characterization of InN on (1 1 1) Ge and c-plane sapphire substrates by RF plasma-assisted molecular beam epitaxy (MBE) are investigated to improve the understanding of InN materials for InN solar cells. n-type InN epitaxial layers were grown on p-Ge and n-Ge substrates to investigate the electrical properties. An epitaxial aluminum (Al) buffer layer was grown on Ge to prevent In–Ge eutectic formation and to replace the tunnel junctions in the tandem solar stacks. We also explore crystalline oxygen in InN/AlN/sapphire films and the possibility of an indium oxynitride compound ($InON_x$). In the following, we specify indium oxynitride as a general non-stoichiometric and/or phase separated material as $InON_x$, in analogy to the nomenclature used for non-stoichiometric silicon nitride (SiN_x).

2. Experimental procedure

InN epitaxial layers were grown by RF plasma-assisted MBE. InN/Ge growth conditions have been published elsewhere [3]. InN materials were grown on (1 1 1) epi-ready Ge and on c-plane sapphire substrates that were solvent cleaned. The Ge and sapphire samples were outgassed in the introduction chamber for 1 h at 320 and 500 °C, respectively. The Ge substrate was then loaded into the growth chamber, where a substrate temperature of 360–475 °C was maintained with an In flux of $0.2–1.4 \times 10^{-7}$ Torr beam equivalent pressure (BEP). Epitaxial Al was deposited on the Ge at different temperatures of 100 and 475 °C. The sapphire substrates were loaded into the growth chamber and nitrided for 1 h with a substrate temperature of 300 °C. Details of the nitridation procedure can be found in Ref. [12]. The InN was grown at a constant substrate temperature of 400 °C with an In flux of $3.47–5.65 \times 10^{-8}$ Torr BEP. Identical plasma power of 350 W, nitrogen flow rates of 0.34 and 0.75 sccm were used for the InN/Al/Ge and InN/AlN/sapphire growths, respectively. Reference samples of AlN/sapphire were also grown and followed the nitridation process described above with a substrate temperature of 200 °C. The AlN was grown at a constant substrate temperature of 800 °C with an Al flux of 1.49×10^{-7} Torr BEP, a plasma power of 350 W, and a nitrogen flow rate of 0.35 sccm. The Al shutter was modulated during growth (10 s of shutter open followed by 10 s of shutter closed.) The crystalline quality of the film was monitored in situ by reflection high-energy electron diffraction (RHEED). Approximately 0.2 μm InN/Al/Ge, 0.4 μm InN/AlN/sapphire, and 0.093 μm AlN/sapphire thick films were grown with a growth rate of approximately 0.2 μm/h for InN and 0.4 μm/h for AlN.

The optical properties of InN/AlN/sapphire were investigated using photoluminescence (PL) measurements at 12 K. Three different experimental setups were conducted to obtain the PL peaks in the visible, infrared (IR), and ultraviolet (UV) region. The excitation pump was provided by a Coherent Innova 300 Ar^+ laser and the pump beam was focused on the sample by conventional optics. A fraction of the backscattered light was collected by conventional optics and was directed into the input slit of an Action Research SpectraPro 2750 monochromator. In the visible region, the pump was tuned to 457.9 nm, with an output power of 100 mW. A charge couple detector (CCD) array that was attached to the side exit of the monochromator was used to detect the spectrally resolved PL signal. In the IR region, the pump was tuned to 514.5 nm, with an output power of 50 mW. In this case, the spectrally resolved signal was diverted to the front exit slit of the monochromator, and was then focused on an InGaAs photodetector by conventional optics. The PL signal from the InGaAs detector was sent to a lock-in amplifier. This provided the ability to use lock-in detection in conjunction with traditional spectral scan to obtain a PL spectrum with high signal to noise ratio. For examining the PL in the UV region, an excitation wavelength of 266 nm was used. This wavelength was achieved by frequency tripling laser pulses at a wavelength of 800 nm. The laser pulses were produced by a Ti:Sapphire laser, and BBO crystals were used to provide the up-conversion. Each of the pulses had a pulse width of approximately 200 fs, and the maximum pulse energy density of the pump was close to 1 mJ/cm^2. The repetition of the pulses was 250 kHz. Using conventional optics, the back-scattered PL emission from the sample was collected and directed to a monochromator. A CCD array was used to detect the spectrally resolved signal from the monochromator.

The electrical properties of n-InN/p-Ge and n-InN/n-Ge junctions were tested by evaporating 400/1000 Å thick Ti/Au on the InN side of the sample patterned by photolithographic means to an area of 0.00456 cm^2. A 1000 Å thick Al layer was evaporated on the entire backside of the Ge wafer to form an ohmic contact. A Keithley 6517 Electrometer was used to measure the *I–V* profiles with the potential bias across the sample increased in uniform time and voltage steps from a minimum, negative value to a corresponding maximum, positive value. A picoammeter was used to read each potential current step for the sample under test. Several measurements were completed on different sections of the wafers to account for growth non-uniformity related variations across the surface of the wafer. The series resistance of the probe-stage setup was also taken into account.

3. Results and discussions

One approach to eliminate the need for degenerate p-type doping, and exploit the ohmic behavior of InN/Ge is with the use of an epitaxial layer of Al as a sub-cell interconnect. This epitaxial Al layer also isolates the Ge from the InN, therefore avoiding the eutectic reaction of In–Ge [3]. The Ge–In eutectic forms at approximately 156 °C [13], well below the growth temperature used in these experiments. The In–Ge eutectic may have been the source of the InN–Ge interfacial layers observed by TEM as shown previously [3]. Fig. 1 shows RHEED images of the crystalline Al deposited on (1 1 1) Ge at different temperatures. Fig. 1(a) was taken of crystalline Al after 60 s deposition at a 100 °C substrate temperature with RHEED images indicating a very spotty pattern. The spotty RHEED pattern became streaky post deposition at an increased substrate temperature of 475 °C, indicating a smooth Al/Ge surface as shown in Fig. 1(b). However, other attempts to deposit Al directly at a 475 °C substrate temperature for 60 s, resulted in persistence of both Al RHEED spots and Ge RHEED streaks as shown in Fig. 1(c); which is indicative of Al droplets not epitaxial Al. Al droplets on these higher deposition temperature samples were confirmed post growth using optical microscopy as shown in Fig. 2.

While epitaxial Al was also chosen to prevent the eutectic of In–Ge, the Al layer may provide domain matching in the Ge–Al–InN interface. Fig. 3 shows the crystallographic alignment of Ge on Al and InN on Al. Every 7th unit cell of Al aligns to within 0.21% to every 8th unit cell of Ge. Every 4th unit cell of InN aligns to every 5th unit cell of Al to within 1%. Therefore, the Al buffer layer while still resulting in highly columnar growth of InN may result in reduced grain tilt of the film. The ability of a film to align based on domain matching is a controversial and possibly incorrect model accounting for the previously demonstrated [3] improved grain alignment as evidenced by X-ray diffraction (XRD). It is included herein for the sake of completeness.

Additionally, the epitaxial Al can act as a collecting junction for tandem solar cells between the different tandem stacks. Current tandem solar cells use tunnel junctions that require degenerate doping to connect the tandem stacks. Research has not been able to demonstrate p-type much less degenerate p-type doping of InN, which is necessary for tunnel junctions. Using the epitaxial Al, creates an interconnecting junction for the p–n tandem stacks. The epitaxial Al is analogous to a wire used to connect a series of diodes. However, the epitaxial Al does not completely remove the need for p-type doping of InN for use in PV applications. p-type InN or p-type InGaN is still needed for the p–n collecting junction tandem stacks.

The crystallographic structure of the InN/Al/Ge was studied by XRD. Fig. 4 shows (ω–2θ) XRD scans for the 0.2 μm thick InN/Al/Ge. Both (0 0 0 2) InN and (1 1 1) Ge diffraction peaks are clearly observed. The (1 1 1) and (0 0 0 2) peak positions were $\theta = 13.581^\circ$ and 15.768° for Ge and InN, respectively. The (0 0 0 2) ω–2θ full-width at half maximum (FWHM) values were ~370 and ~276 arcsec for InN on Ge and Al/Ge substrates, respectively. It is clearly seen that the epitaxial-Al buffer layer did not inhibit the growth of InN.

I–V curves of n-InN/p-Ge and n-InN/n-Ge show ohmic behavior with a series resistance range of approximately 5–8 Ω/cm^2, as shown in Fig. 5. This series resistance shows no contribution from the InN or the electrode InN interface, equating to the Ge bulk series resistance. Both n-Ge and p–Ge show no noticeable rectifying behavior even though the Fermi energy differs by approximately 0.6 eV. This implies strong band bending at the InN–Ge junctions as observed elsewhere at the InN free surface [9–11]. Therefore, because n-InN/p-Ge and n-InN/n-Ge show ohmic behavior, traditional methods of designing tandem solar cells will not be applicable.

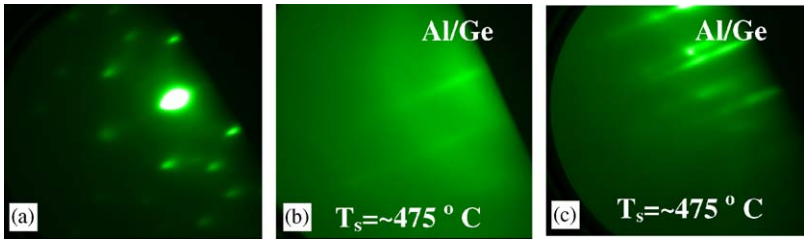

Fig. 1. RHEED images of Al/Ge. (a) Crystalline Al after 60 s on Ge at 100 °C; (b) Al on Ge after substrate temperature increased from 100 to 475 °C; (c) crystalline Al after 60 s on Ge at 475 °C.

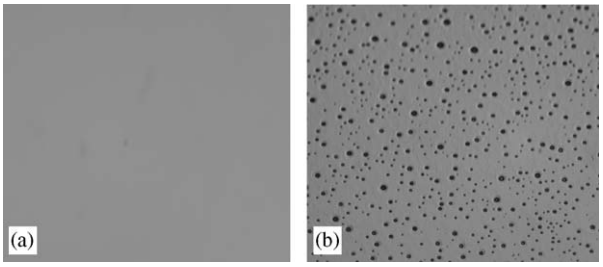

Fig. 2. Microscopic image of (a) Al/Ge deposited at 100 °C and (b) Al/Ge deposited at 475 °C.

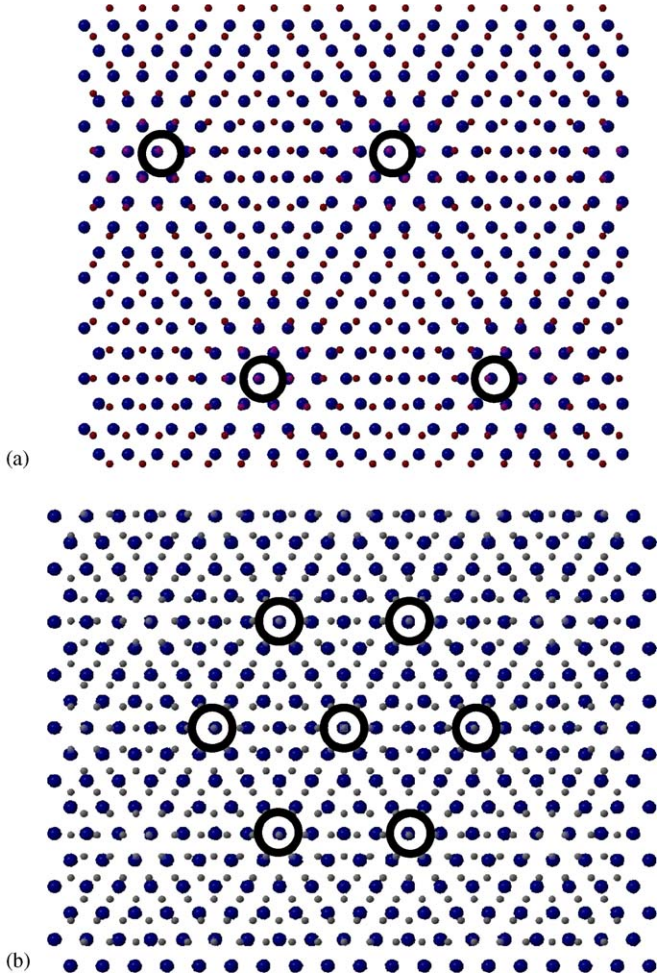

Fig. 3. Crystallographic alignment of (a) Ge (large dots) and Al (small dots); (b) InN (large dots) and Al (small dots); the circles indicate domain matching.

The recent discovery of a lower bandgap of InN has sparked a debate into the origin of the higher quoted bandgap value. It is believed that the higher value is related to the presence of oxygen, previously thought to be present as an alloy. Although, more recently it has been suggested that a discrete oxynitride compound or compounds is a better interpretation than that of an alloy [6,14–16]. During one series of experiments a vacuum window was slightly breeched resulting in a very small leak that raised the MBE

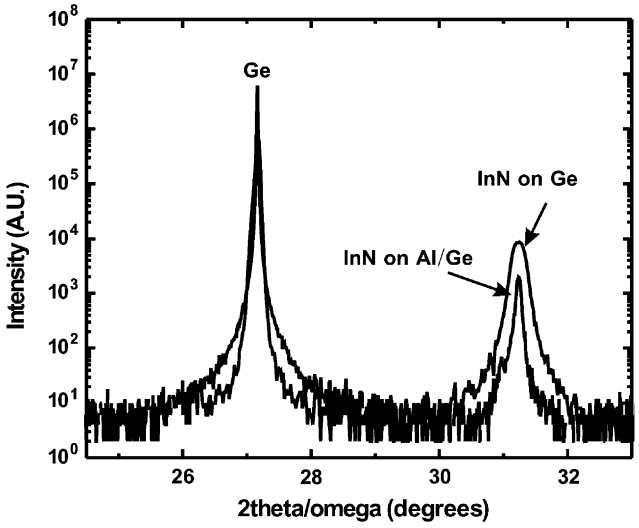

Fig. 4. $2\theta/\omega$ XRD scan of InN/Al/Ge showing Ge peaks at 13.581° and InN peaks at 15.768°.

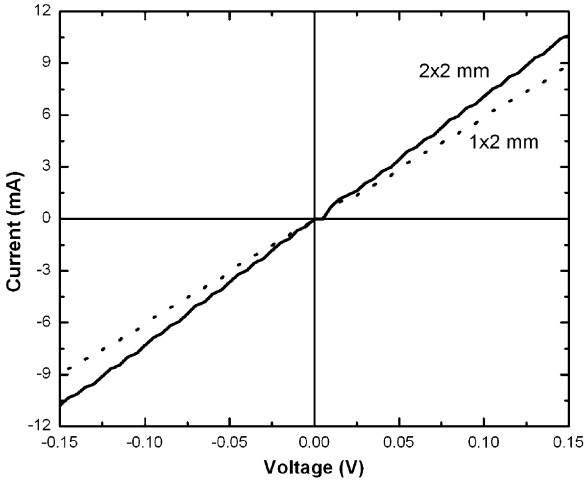

Fig. 5. *IV* curves on n–InN/p–Ge for 1×2 mm (dotted) and 2×2 mm (solid).

system base pressure from $\sim 1 \times 10^{-10}$ to $\sim 1 \times 10^{-9}$ Torr over the course of several growths. This minute level of leak would not be detectable in growth technologies where ultra high vacuum conditions are not used. Therefore, the following results emphasize the sensitivity of InN to extremely low levels of oxygen contamination. In these series of samples, it was determined that there was unintentional in situ oxygen incorporation in the InN films of increasing magnitude as the leak worsened. Evidence of oxygen was found while studying the crystallographic structure of the InN/AlN/sapphire sample by XRD. Fig. 6 shows the (ω–2θ) scan of this sample. The peaks observed in Fig. 6 occur at $2\theta = 30.874°$ and 31.158°. The higher angle peak clearly matches hexagonal InN but the lower angle peak does not match cubic InN, cubic In_2O_3, or metallic In and is only found in material grown when the leak was present in the MBE system. However, as

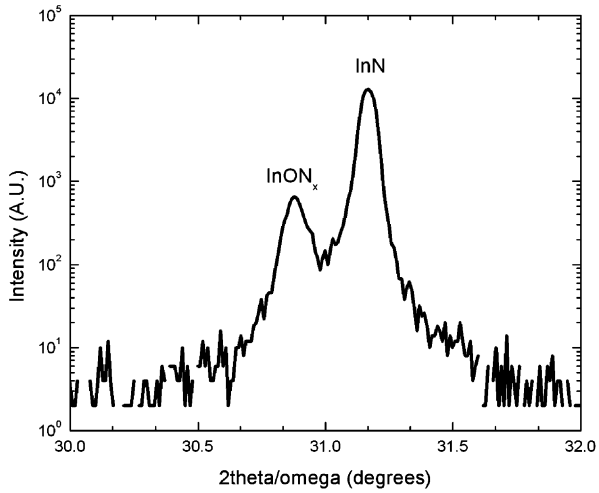

Fig. 6. $2\theta/\omega$ XRD scan of InN/AlN/sapphire showing an InON$_x$ peak at 15.437° and an InN peak at 15.579°.

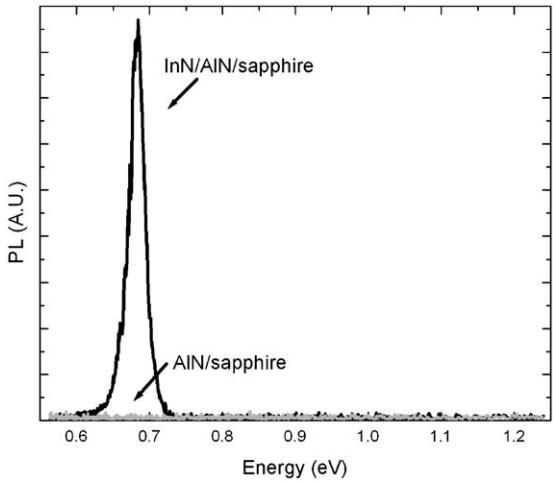

Fig. 8. PL of InN/AlN/sapphire (black line) and AlN/sapphire (light grey line) taken at 12 K with peak intensity at ~0.7 eV.

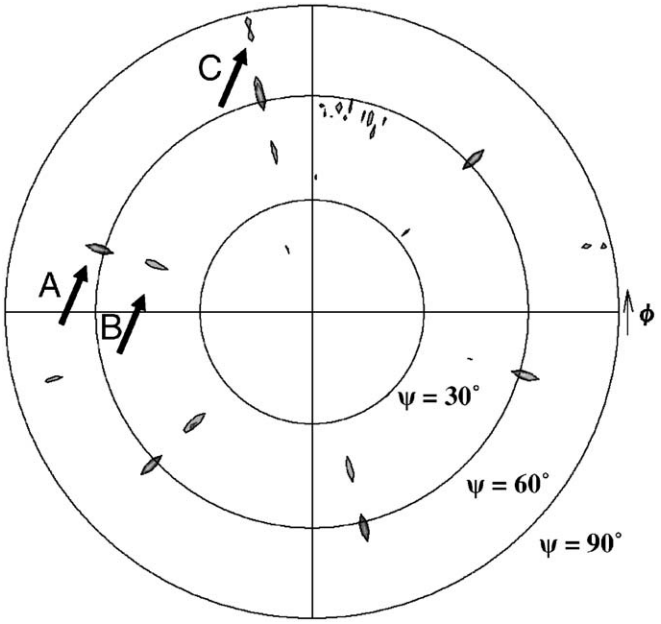

Fig. 7. Pole figure of InN/AlN/sapphire showing hexagonal sapphire peaks ⟨1 1 3⟩, hexagonal InN peaks ⟨1 0 2⟩, and cubic InON$_x$ ⟨4 2 2⟩, labeled A, B, and C, respectively. is the angle relative to the normal surface.

this new peak is in between the cubic InN and cubic In_2O_3 peaks it is tentatively assigned as an indium oxynitride material of yet to be determined stoichiometry. As to emphasize the unknown and possible non-stoichiometric nature of this material, we will describe this material as InON$_x$. Fig. 7 shows the pole figure of this sample showing evidence of hexagonal ⟨1 0 3⟩ InN (labeled B) that is 30° rotated with respect to the ⟨1 1 3⟩ sapphire substrate (labeled A) and the presence of a cubic material, possibly ⟨4 2 2⟩ InON$_x$ (90° symmetric peaks labeled C). However, upon examination of previous samples grown under conditions of higher than normal base pressure, indicative of an increasing magnitude leak, (ω–2θ) scans did not show any indication of peaks related to InON$_x$. However, these same samples not showing ω–2θ indium oxynitride peaks did show cubic InON$_x$ ⟨4 2 2⟩ diffraction peaks when a pole figure was measured indicating the ⟨4 2 2⟩ reflection is a sensitive measure of the existence of mixed indium oxynitrides.

Fig. 8 shows the PL spectrum of the InN epitaxial layer grown on an AlN buffer layer on a sapphire substrate and a reference sample of an epitaxial AlN layer grown on a sapphire substrate. PL was observed at a peak centered at 1771 nm, corresponding to approximately 0.7 eV for the InN/AlN/sapphire sample and no contribution from the AlN/sapphire reference sample. Fig. 9 also shows the PL spectrum of the previously mentioned InN/AlN/sapphire and reference AlN/sapphire, along with InN/Ge and a bare Ge wafer. The InN/AlN/sapphire and AlN/sapphire sample have an observed narrow peak at 700 nm, corresponding to approximately 1.77 eV. This PL energy is thought to be consistent with emission from the sapphire substrate [17] and should not be confused with the reported PL from InN as the AlN/sapphire sample contains no InN. Additionally, the InN/Ge sample shows no PL at all in this range. Fig. 10 shows the UV PL spectrum for the same set of samples used in Fig. 9. As shown in the graph, the InN/AlN/sapphire sample has a peak intensity measured at 330 nm, corresponding to approximately 3.8 eV. As previously mentioned, this InN/AlN/sapphire sample was grown under a leaky MBE environment and from XRD ω–2θ, an InON$_x$ film was found. It is thought that the InON$_x$ film is the cause of the 3.8 eV PL peak. From the literature, In_2O_3 has a know bandgap of 3.75 eV [18]. Also shown in Fig. 10, there is no significant emission from the AlN/sapphire sample, InN/Ge sample or bare Ge wafer. Additionally, the peaks in the visible, IR, and UV range used different optical configurations. Therefore, the output data was multiplied to achieve a comparable intensity leading to arbitrary units for the PL intensity.

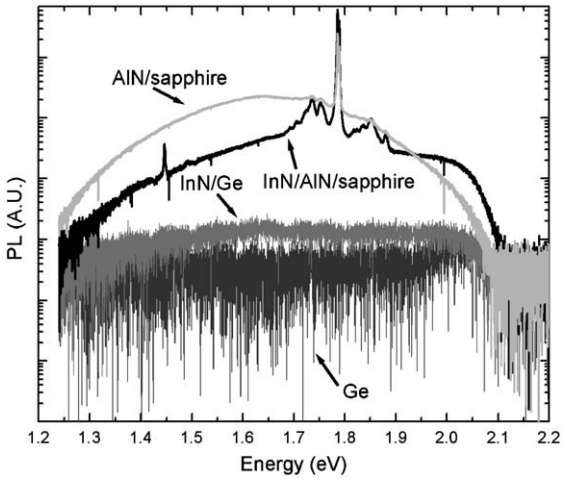

Fig. 9. PL of InN/AlN/sapphire (black line), AlN/sapphire (light grey line), bare Ge wafer (dark grey line), and InN/Ge (grey line) taken at room temperature with peak intensities at ~1.77 eV.

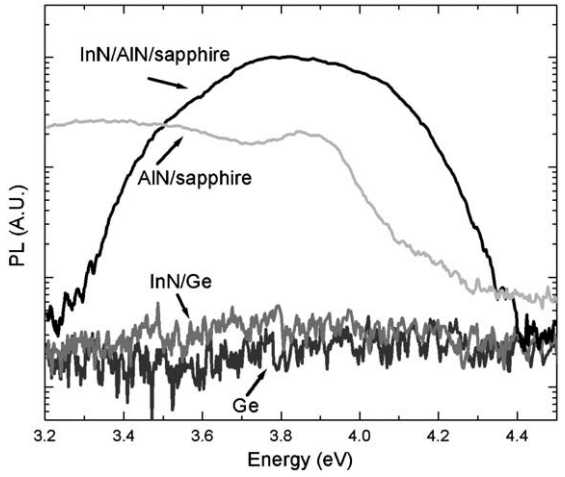

Fig. 10. PL of InN/AlN/sapphire (black line), AlN/sapphire (light grey line), bare Ge wafer (dark grey line), and InN/Ge (grey line) taken at room temperature with peak intensity at ~3.8 eV.

The results in Figs. 9 and 10 provide another insight into the argument of the bandgap value of InN and the origin of the 1.7–1.9 eV bandgap. As mentioned previously, the peak found for our InN/AlN/sapphire at ~1.7 eV is related to emission from the sapphire substrate. A similar 1.7 eV PL peak was not found on InN/Ge samples or on bare Ge wafers. Although PL is not a definitive measure of bandgap, as emission can results from multiple sources including deep levels, a possible explanation for the origin of the higher InN bandgap could be the contribution from the sapphire substrate from pump absorption or merely sapphire emission. Further research into this matter is required.

Annealing pure InN films in oxygen has determined that high-quality wurtzite InN has a strong affinity for incorporating oxygen into the crystal structure after thermal treatments in air [14,16]. Moreover, Davydov et al. [6] state that samples saturated partially with oxygen show a shift towards higher bandgap energies than that of untreated InN. It is believed that the incorporation of oxygen may play a key role in determining the apparent properties of InN including the bandgap and the lattice constant. The results presented herein add to this data, indicating that small oxygen exposure during growth does not shift the PL peak from approximately 0.68 eV. However, there is evidence of an oxynitride related phase as determined from XRD.

4. Conclusion

Several key aspects of InN for use in photovoltaic applications are described. While offering potential for solar cells, several key issues including p-type doping and rectifying solid state junctions have yet to be demonstrated. An investigation of InN grown on Ge and sapphire substrates via plasma assisted MBE was carried out to study the material characteristics of InN for its use in PV devices. The bandgap of InN was determined to be approximately 0.7 eV. However, an additional, higher-energy PL emission of approximately 1.6 and 3.8 eV was observed for InN material grown on a sapphire substrate and under a leaky MBE environment. The 1.6 eV PL emission is possibly due to pump absorption or sapphire emission from the sapphire substrate. Based on the X-ray diffraction results, the 3.8 eV bandgap energy is possibly related to $InON_x$, or a highly degenerate surface layer. For the development of InN tandem solar cells, a new interconnection method using epitaxial Al layers, which can be used to interconnect p–n InN junctions was demonstrated. Further research continues on p-type InN, along with current technical issues related to implementing InN/InGaN tandem solar cell devices.

Acknowledgments

This work was supported by the Office of Navel Research monitored by Dr. Colin Wood and the Department of Energy–National Renewable Energy Lab monitored by Dr. Bob McConnell. The authors would like to thank Dr. William Schaff from Cornell University for his unique insight and helpful comments on the growth of InN.

References

[1] V.Yu. Davydov, A.A. Klochikhin, R.P. Seisyan, V.V. Emtsev, S.V. Ivanov, F. Bechstedt, J. Furthmüller, H. Harima, A.V. Mudryi, J. Aderhold, O. Semchinova, J. Graul, Phys. Status Solidi B 229 (2002) R1.
[2] J. Wu, W. Walukiewicz, K.M. Yu, J.W. Ager III, E.E. Haller, H. Lu, W.J. Schaff, Y. Saito, Y. Nanishi, Appl. Phys. Lett. 80 (2002) 3967.
[3] E. Trybus, G. Namkoong, W. Henderson, W.A. Doolittle, R. Liu, J. Mei, F. Ponce, M. Cheung, F. Chen, M. Furis, A. Cartwright, J. Crystal Growth 279 (2005) 311.
[4] S. Strite, H. Morkor, J. Vac. Sci. Technol. B 10 (1992) 1237.
[5] T.L. Tansley, C.P. Foley, J. Appl. Phys. 59 (1986) 3241.
[6] V.Y. Davydov, et al., Phys. Stat. Sol. B 234 (2002) 787.

[7] J. Wu, W. Walukiewicz, W. Shan, K.M. Yu, J.W. Auger III, E.E. Haller, H. Lu, W.J. Schaff, Phys. Rev. B 66 (2002) 201403.
[8] R.R. King, et al., Proceedings of the third World Conference of Photovoltaic Energy Conversion, Japan, 2003, pp. 622–625.
[9] T.D. Veal, I. Mahboob, F.J. Piper, C.F. McConville, H. Lu, W.J. Schaff, J. Vac. Sci. Technol. B 4 (2004) 2175.
[10] I. Mahboob, T.D. Veal, C.F. McConville, Phys. Rev. Lett. 92 (2004) 036804.
[11] K.A. Ricket, A.B. Ellis, F.J. Himpsel, H. Lu, W. Schaff, J.M. Redwing, F. Dwikusuma, T.F. Kuech, Appl. Phys. Lett. 82 (2003) 3254.
[12] G. Namkoong, W.A. Doolittle, A.S. Brown, M. Losurdo, M.M. Giangregorio, G. Bruno, J. Crystal Growth 252 (2003) 159.
[13] A.J. McAlister, J.L. Murray, Binary Alloy Phase Diagrams, second ed, ASM International, Metals Park, 1990, p. 1956.
[14] T. Yodo, Y. Kitayama, K. Miyaki, H. Yona, Y. Harada, K.E. Prince, K.S.A. Butcher, J. Crystal Growth 269 (2004) 145.
[15] M. Yahimoto, H. Yamamoto, W. Huang, H. Harima, J. Saraie, A. Chayahara, Y. Horino, Appl. Phys. Lett. 82 (2003) 3480.
[16] E. Kurimoto, M. Hangyo, H. Harima, M. Yashimoto, T. Yamaguchi, T. Araki, Y. Nanishi, K. Kisoda, Appl. Phys. Lett. 84 (2004) 212.
[17] N. Kristianpoller, A. Rehavi, A. Shmilevich, D. Weiss, R. Chen, Nucl. Instrum. Methods Phys. Res. B 141 (1998) 343.
[18] I. Hamberg, C.G. Granqvist, J. Appl. Phys. 60 (1986) R123.